

Aerosol characterization using satellite remote sensing of light pollution sources at night

Miroslav Kocifaj,^{1,2*} Salvador Bará,³

¹*Faculty of Mathematics, Physics, and Informatics, Comenius University, Mlynská dolina, 842 48 Bratislava, Slovakia*

²*ICA, Slovak Academy of Sciences, Dúbravská cesta 9, 845 03 Bratislava, Slovakia*

³*Departamento de Física Aplicada, Universidade de Santiago de Compostela, 15782 Santiago de Compostela, Galicia, Spain*

Accepted XXX. Received YYY; in original form ZZZ

ABSTRACT

A demanding challenge in atmospheric research is the night-time characterization of aerosols using passive techniques, that is, by extracting information from scattered light that has not been emitted by the observer. Satellite observations of artificial night-time lights have been used to retrieve some basic integral parameters, like the aerosol optical depth. However, a thorough analysis of the scattering processes allows one to obtain substantially more detailed information on aerosol properties. In this Letter we demonstrate a practicable approach for determining the aerosol particle size number distribution function in the air column, based on the measurement of the angular radiance distribution of the scattered light emitted by night-time lights of cities and towns, recorded from low Earth orbit. The method is self-calibrating and does not require the knowledge of the absolute city emissions. The input radiance data are readily available from several spaceborne platforms, like the VIIRS-DNB radiometer onboard the Suomi-NPP satellite.

Key words: light pollution – scattering – radiative transfer – atmospheric effects – instrumentation: photometers

1 INTRODUCTION

Determining the aerosol properties at night-time is an essential step for a better understanding of aerosol dynamics, with direct applications to the study of planetary atmospheres, the characterization of potential candidate sites for astrophysical observatories, and light pollution research. Artificial night lights of cities and towns offer a permanent set of light beacons distributed worldwide, whose observation from Earth orbiting platforms has been shown to be useful to determine some basic integral properties of the aerosols contained in the air column, as e.g. the aerosol optical depth (Choo and Jeong 2016; Johnson et al. 2013; McHardy et al. 2015; Wang et al. 2016; Zhang et al. 2008, 2019). However, night-time imagery contains additional useful information, among other the angular dependence of the signal produced by the artificial light scattered by the atmosphere, that can be measured in clear and moonless nights by observing the radiance received at the satellite from directions corresponding to Earth pixels with no light sources, preferably located in the vicinity of urban nuclei with sharp geographical borders. This scattered light appears in the satellite images as a diffuse glow surrounding the city areas, blurring the city

limits, and with decreasing radiance for increasing distances (e.g. Sánchez de Miguel et al. 2019). In this Letter we show that the specific way in which the scattered radiance varies with the nadir angle of the observed pixels, as seen from the satellite radiometers, can be used to retrieve more specific key aerosol properties like e.g. their particle size number distribution function, if some additional *a-priori* information is available. An important feature of this approach is that it is self-calibrating: since it is based on the analysis of the angular dependence of the scattered radiances normalized to the direct radiance received from the city, the knowledge of the absolute emissions from the urban area is not required for its application.

2 THE MODEL

A light source seen in satellite imagery of an atmosphereless planet would be geometrically sharply confined. However, due to light scattering by atmospheric constituents, the brightness of the artificially lit surface of the Earth at night does not change abruptly when transitioning from bright image pixels to neighbouring pixels at the outer interface of a city or town. Normally the radiance of a surface decreases steeply but in a continuous way, as the angular distance

* E-mail: kocifaj@savba.sk

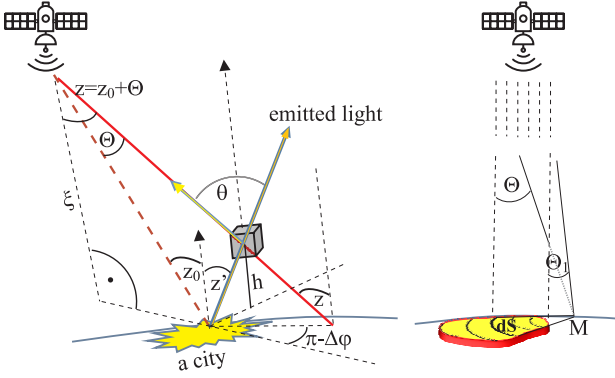


Figure 1. Scattering geometry for: (a)(left plot) remote sensing away from the satellite vertical direction, (b)(right plot) satellite at near zero zenith angle from the city. The parameters shown in the figure are described in the main body of the text.

from the city-edge increases, while quickly approaching the background level.

The radiance of the Earth's surface, $R_S(z)$, reaching the satellite sensor can be computed as the integral of elementary optical signals produced from light scattering in the atmospheric volumes along the line of sight (see Fig. 1a)

$$R_S(z) = \frac{1}{\cos z} \int_{h=0}^{\xi} dI_0(z') \exp \left\{ -\frac{\tau(h)}{\cos z} - \frac{\tau(0) - \tau(h)}{\cos z'} \right\} \tilde{\omega} k_{ext}(h) \frac{\cos^2 z'}{h^2} \frac{p(\theta)}{4\pi} dh, \quad (1)$$

where $z \approx z_0 + \Theta$ is the zenith angle of a surface area in the city surroundings that has no light sources, while z_0 is the zenith angle of an illuminated surface element within the city or town. In Fig. 1a Θ is the angle between the direction of observation and the position of a point source of light (or a surface element dS of an artificially lit area). The normalized scattering phase function $p(\theta)/(4\pi)$ shapes with the scattering angle θ

$$\cos \theta = \cos z \cos z' + \sin z \sin z' \cos(\Delta\varphi). \quad (2)$$

The angles z , z' and $\Delta\varphi$ are defined in Fig. 1a. In Eq. 1 the product of the single scattering albedo, $\tilde{\omega}$, and the volume extinction coefficient, k_{ext} , is known as the atmospheric volume scattering coefficient (see e.g. Kokhanovsky 1998). The optical thickness $\tau(h)$ is calculated for an atmospheric column that extends from altitude h to the satellite level ξ , i.e. $\tau(h) = \int_h^{\xi} k_{ext}(h') dh'$. Finally, $dI_0(z')$ is the radiant intensity (measured in Wsr^{-1}) emitted by an elementary area dS of the city, that can be expressed as

$$dI_0(z') = \tilde{R}_0(z') dS, \quad (3)$$

where $\tilde{R}_0(z')$ has the units of radiance ($Wm^{-2}sr^{-1}$). The radiant intensity emitted by a city normally depends on the emission angle z' . The collective effect of differently oriented and sloped surfaces, however, is that the intensity usually varies slowly with z' . This is consistent with the models currently in use (e.g. Fig. 5 in Koll  th and Kr  nicz 2014). The angular dependences of the remaining terms in the integrand in Eq. 1 are much more pronounced, e.g. $p(\theta)$ shows a dramatic decrease rate by one or more orders of magnitude across its definition domain, with a typical strong forward

lobe and a weak side scattering. After a considerable manipulation of mathematical expressions (not shown here) we obtain

$$R_S(\Theta) = \frac{\tilde{R}_0 e^{-\tau(0)}}{(\xi \sin \Theta)^2} dS \left(\frac{\lambda}{2\pi} \right)^2 \int_0^{\xi} \left[\int_0^{\infty} S_{11}(a, z') f(a, h) da \right] \sin^2(z') dh, \quad (4)$$

for the angular dependence of the scattered radiance detected by the satellite at wavelength λ . In this equation it is assumed that the satellite passes almost vertically over the city (i.e. at near zero zenith angle), and that the radiant intensity emitted by the city is slowly dependent on z' , having an average value $\tilde{R}_0 dS$. Due to atmospheric extinction the radiance of the bright pixels is reduced to $\tilde{R}_{0\xi} = e^{-\tau(0)} \tilde{R}_0$ when measured at the satellite level. The approximations used in deriving the above formula also comprise i) $\theta \approx z' + \Theta \approx z'$, ii) $z = \Theta$, iii) the contribution of Rayleigh scattering to the radiance recorded at satellite level for $\Theta \lesssim 0.09^\circ$ is much smaller than the one from aerosols (see Fig. 2), and iv) the Mie theory for spherical homogeneous particles of radii a controls the far-field scattering amplitude through the first element of the scattering matrix, S_{11} , which is also known as the scattering function. The scattered signal from an ensemble of independent particles is proportional to the product of $S_{11}(a, z')$ and $f(a, h)$, where the latter is the particle size number distribution function, i.e. the number of particles per unit volume having radii between a and $a + da$ at height h above ground level. More accurately, when vegetation and city structures or outdoor luminaire designs are all not efficient enough in blocking light emissions to low elevation angles, an exponential term should be kept in Eq. 4, i.e.

$$R_S(\Theta) = \frac{\tilde{R}_{0\xi}}{(\xi \sin \Theta)^2} dS \left(\frac{\lambda}{2\pi} \right)^2 \int_{h=0}^{\xi} \exp \left\{ [\tau(0) - \tau(h)] \left(1 - \frac{1}{\cos z'} \right) \right\} \int_{a=0}^{\infty} S_{11}(a, z') f(a, h) \sin^2(z') da dh \quad (5)$$

The radiance $R_S(\Theta)$ increases steeply when Θ approaches zero, and we evidence in Fig. 2 that the aerosol contribution is dominant (in comparison with Rayleigh's molecular one) in shaping the radiance patterns for almost all emission angles z' and for most typical values of the aerosol asymmetry parameter g . The latter is commonly used in radiative transfer theories to characterize the average cosine of the scattering angle, assuming that the probability of a photon to be scattered per unit solid angle around the direction z' is proportional to the phase function $p(z')$. In the numerical demonstration we have varied the asymmetry parameter in order to model different aerosol types. Values of g approaching unity usually indicate the presence of large particles with a strong forward scattering lobe, while $g \approx 0$ corresponds to isotropically scattering media containing particles much smaller than the spectral detection range (e.g. Moosm  ller and Ogren 2017). Most typically, g ranges from a few tenths to ≈ 0.9 . This is why the numerical demonstration of aerosol contribution to the satellite radiance is performed for $g=0.3 \dots 0.9$.

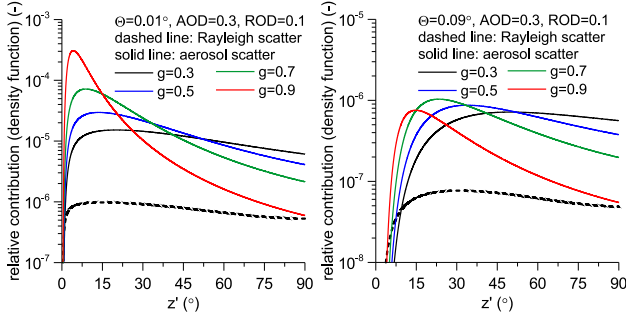


Figure 2. The contributions from aerosol and Rayleigh scatterings to the radiance at satellite level, shown as a function of the emission angle z' (see Fig. 1a). Left plot (a) is for $\Theta = 0.01^\circ$, while the right plot (b) is for $\Theta = 0.09^\circ$. The aerosol populations under analysis differ in the asymmetry parameter, g , which can theoretically range from -1 (entirely backscattered light) to 1 (scattered light directed exclusively in the forward direction). Negative values of g are scarcely observed in nature. ROD is the Rayleigh Optical Depth, while AOD is the Aerosol Optical Depth.

3 THE INVERSE SCATTERING PROBLEM

For a satellite located at near zero zenith angle above the city and $\theta \approx z'$ we have $dh \sin^2 z' = -\xi \sin \Theta dz'$, while the mapping from the space of experimental radiance data, $R_s(\Theta)$, to the space of particle size distribution functions $f_0(a)$ is described by the following integral equation

$$\frac{R_S(\Theta_1)}{\tilde{R}_{0\xi}} = \int_{a=0}^{\infty} f_0(a) K_{S11}(\Theta_1, a) da \quad (6)$$

where Θ_1 is the smallest angular separation between the bright surface area of a city and the direction of remote sensing, and $R_S(\Theta_1)$ is the radiance scattered towards the satellite from the whole atmospheric column along the line of sight ending in point M (see Fig. 1b). For a vertically stratified atmosphere $f(a, h) = f_0(a)F(h)$, where $F(h)$ is commonly approximated by an exponential function $F(h) = \exp\{-h/H_A\}$ with H_A being the aerosol scale height (e.g. Waquet et al. 2007). In most cases H_A ranges from 1 to 3 km. The kernel $K_{S11}(\Theta_1, a)$ of the integral equation has the following form for the satellite remote sensing of a light pollution source

$$K_{S11}(\Theta_1, a) = 2\xi \left(\frac{\lambda}{2\pi}\right)^2 \int_{\Theta_1}^{\Theta_1+\Delta\Theta} \epsilon(\Theta) \int_{z'=0}^{\pi/2} S_{11}(a, z') \exp\left\{\frac{\xi \sin \Theta}{H_A \tan z'}\right\} dz' d\Theta \quad (7)$$

where $\Delta\Theta = \Theta_N - \Theta_1$ is the angular span between the nearest and farthest bright areas in the city, measured from the point M in the satellite images (cfr. Fig. 1b). $\epsilon(\Theta)$ is the half-angle subtended by each elementary arc of the city emitting area, as seen from the ground point M , for each value of Θ (see arcs within dS in Fig. 1b). The inverse problem consists in finding the solution vector $f_0(a)$ that, for a given $K_{S11}(\Theta_1, a)$, produces the best match to the experimentally determined data vector $R_S(\Theta_1)/\tilde{R}_{0\xi}$. The retrieval of the particle size number distribution function from Eq. 6 can be difficult because the problem is typically ill-posed until additional (*a-priori*) information on the aerosols can be applied.

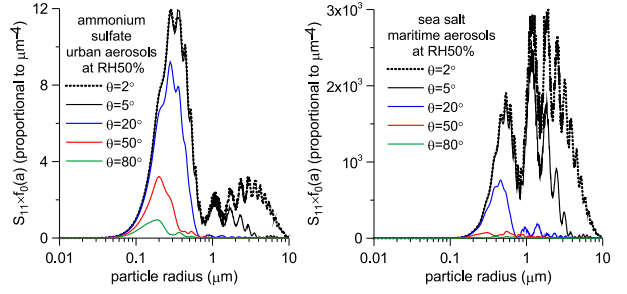


Figure 3. Relative contribution of different particle radii to the elementary radiance at a set of scattering angles θ and for relative humidity at about 50%. Left plot (a) is for ammonium sulfate (urban-like) aerosols. Right plot (b) is for sea salt (maritime) particles.

For instance, the material composition is one of the important properties that predetermine the range of applicability of the inverse transform. For urban, industrial-like aerosols with refractive index as described in (Kent et al. 1983) we have found that the peak contribution to the scattered signal is due to submicrometer-sized particles at almost all scattering angles θ (see Fig. 3a). On the other hand, the contribution from micrometer-sized particles to the scattered signal is also important if e.g. humidified sea salt is present in the atmosphere (see Fig. 3b). This implies that the method is neither sensitive to very small particles with size parameter $x = 2\pi a/\lambda \lesssim 1$ nor to particles larger than a few micrometers. The traditional solution to the Fredholm integral equation (Eq. 6) is to implement some suitable regularization algorithm, but the problem can be significantly simplified by reducing the number of unknowns. For instance, instead of searching for a N -element solution vector $f_0(a_i)$ ($i = 1..N$), an alternative and more efficient approach consists in using a parametric analytical model for the particle size number distribution function and determining its free parameters by minimizing a cost function, especially if the number of these unknown parameters is low. Ideally e.g. a log-normal distribution with two shaping parameters (the particle modal radius r_m and the size-distribution width σ) may allow for transitioning from a complex inversion problem to a simple minimization one.

4 PROCESSING THE VIIRS-DNB NIGHTTIME LIGHT IMAGERY OF ZARAGOZA CITY

We present in this section a proof-of-concept of the application of this approach to obtain the columnar particle size number distribution function $\hat{f}_0(a) = \int_0^\infty f(a, h) dh = H_A f_0(a)$ by inverting Eq. 6 with the kernel given in Eq. 7. We used as input data the radiances $R_S(\Theta_1)$ and $\tilde{R}_{0\xi}$ measured by the VIIRS-DNB radiometer onboard the Suomi-NPP satellite during its pass over the city of Zaragoza (Spain, 41.65 N, 0.89 W) in the night of July 5th, 2019 at 03:59 CEST (01:59 UTC). This pass took place in a clear and moonless night, with the Moon at 30.14 degrees below the horizon, illuminated at 7.2 per cent, and Sun altitude -20.6 degrees, at the time of the measurements. That night

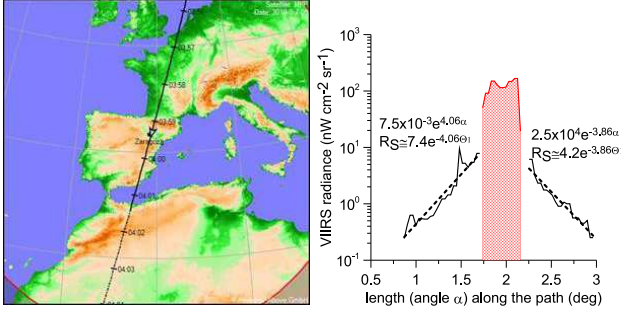


Figure 4. Left plot (a): projection of the Suomi-NPP satellite's orbit onto the surface of the Earth (ground track), during its pass over Zaragoza (Spain) in the night of July 5, 2019 (Peat 2020). Right plot (b): The radiance as a function of the nadir angle α (measured in degrees, as seen from the satellite). The radiance has been taken at two edges for the first and the last contacts with the artificially lit surface area of the city. Red color is for the inner parts of the city.

the satellite passed almost vertically over the city, at an altitude of 89 degrees over the horizon, corresponding to a zenith angle $z_0 = 1^\circ$ (see Fig. 1a, and ground track in Fig. 4a).

The Suomi-NPP satellite, launched on October 2001, is located in a polar sun-synchronous orbit of 826 x 828 km, with an inclination of 98.7°, recording the Earth radiance in a panchromatic band (500-900 nm), with 14-bit quantization and a low light imaging detection limit of $5 \times 10^{-11} \text{ W cm}^{-2} \text{ sr}^{-1}$ (Cao and Bai 2014; Elvidge et al. 2013, 2017). The radiance data are available as geotiff files in the WGS84 coordinate reference system, with pixel size of 15 arcseconds, measured from the center of the Earth (NOAA 2019). This corresponds to a pixel angular size of about $\Delta\Theta=115$ arcseconds in the North-South direction, as seen from the satellite location at low nadir angles. The radiance pixel array analyzed in our study was taken along a North-South path passing through the urban center, which provides the $\tilde{R}_{0\xi}$ values, and encompassing large unpopulated segments of territory at its extremes, where the recorded $R_S(\Theta_1)$ radiance is mostly due to atmospheric scattering. Zaragoza has a compact urban structure with well defined city limits, subtending, from the satellite, an angle of order 0.58 degrees. The average value $\tilde{R}_{0\xi}$ can be obtained from the radiance recorded within the city (see Fig. 4b, red line). The values of $R_S(\Theta_1)$ are measured from the city border, obtaining in this way two sub-arrays of measurements along the path, one before reaching the North border of the city and other starting from the South border (Fig. 4b, full black lines). The dashed black lines in Fig. 4b are logarithmic fits of the raw radiance, removing the small local peaks associated with some residual sparse sources of light.

Two instrumental data arrays can be immediately computed from these measurements: the ratio $R_S(\Theta_1)/\tilde{R}_{0\xi}$, and the kernel $K_{S11}(\Theta_1, a)$ (according to Eq. 7). These arrays are the required inputs for performing the inversion of Eq. 6 in order to obtain the estimate $\tilde{f}_0(a)$. This inversion can be carried out using different approaches. One of them is to perform a conventional linear estimation with an appropriate Tikhonov's regularization parameter. Another useful procedure consists on the choice of a suitable analytic form for $\tilde{f}_0(a)$, based on the available *a-priori* knowledge about

the physical properties of the phenomenon under study, and determining the unknown parameters of this trial function by using conventional minimization routines. In this work we resorted to the latter option, by assuming that the particle size number distribution function can be well described by the linear combination of a set of $i=1\dots M$ log-normal distributions in the form

$$\tilde{f}_0(a) = \sum_{i=1}^M \frac{N_i}{\sigma_i a} \exp \left\{ -\frac{1}{2} \frac{[\log_{10}(a) - \log_{10}(a_i)]^2}{\sigma_i^2} \right\} \quad (8)$$

where each i -th distribution is characterized by a small set of parameters (a_i, σ_i, N_i) , informing about its position and width on the particle size space, and its relative weight in the linear combination, respectively. Ideally a low number of elementary distributions ($M=1$ or 2) should be enough for building up a good approximation to $\tilde{f}_0(a)$. Some additional *a-priori* knowledge may be used to improve the estimation. Zaragoza is located in the mid of a semi-arid zone, so that dust-like particles make an important part of the total aerosol content. The characteristic refractive index of dust-like particles, $1.52+0.025i$, can be potentially influenced by humidity at night, so we used a reduced index of $1.4+0.002i$. With these assumptions we minimized the quadratic differences between the measured radiance ratios, $R_S(\Theta_1)/\tilde{R}_{0\xi}$, and those expected from Eq. 8 (substituted into Eqs. 6 and 7) with respect to the unknown parameters a_i, σ_i, N_i ($M=2$), avoiding too narrow and too wide widths (σ_i), as well as to small and too large modal radii a_i . The computations were made for $\lambda = 650$ nm, the weighted average wavelength of the VIIRS-DNB spectral sensitivity band.

Incorporating all these constraints we obtain $N_1/N_2 \approx 125$, $a_1 \approx 0.08 \mu\text{m}$, $\sigma_1 \approx 0.15$, $a_2 \approx 0.5 \mu\text{m}$, and $\sigma_2 \approx 0.3$. The resulting particle distribution function is shown in form of the volume density function (Fig. 5b) to be consistent with presentation form of the AERONET data products. Fig. 5a shows that the best match of the theoretical model (Eq. 4) to the experimental data occurs for AOD ≈ 0.3 . The $R_S(\Theta_1)/\tilde{R}_{0\xi}$ ratio as a function of Θ_1 becomes steeper for larger AODs, and more flat for lower AODs. In addition, the absolute values of $R_S(\Theta_1)/\tilde{R}_{0\xi}$ increase with increasing AOD, so one can easily estimate the optimum AOD for the time of measurement. These results are fairly similar to those reported by the AERONET station located in Zaragoza (41.63 N, 0.88 W, height=250 m) a few hours after the Suomi-NPP pass (NASA 2020): the recorded AOD at 05:45 UTC for $\lambda=675$ nm was 0.3, and the retrieved particle size volume distribution function clearly shows the same bimodal structure predicted in Fig. 5b, a feature of the aerosol distribution that was maintained along that day. The two peaks of that function at 06:07 UTC, first available data for this day, were centered in aerosol particle radii slightly above 0.1 and 2 μm , with maximum values close to 0.035 and 0.13 $\mu\text{m}^3 \mu\text{m}^{-2}$, respectively. The peak locations are similar, and the peak values are of the same order of magnitude but slightly lower than those deduced from the VIIRS-DNB images. Some differences could be expected, since the VIIRS-DNB measurements were obtained at 01:59 UTC, a few hours before dawn.

Let us point out that the actual particle volume distribution function is not expected to be as smooth as that displayed in Fig. 5b. The smoothness of this estimate comes from the fact that it has been obtained using a linear com-

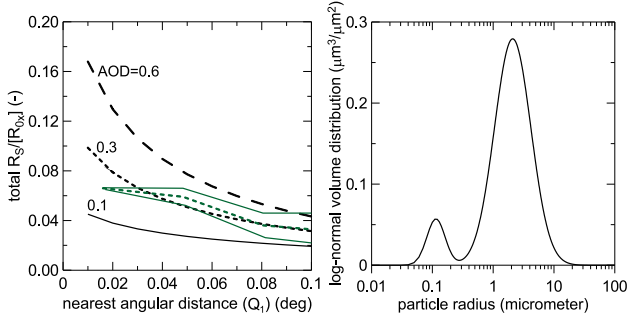


Figure 5. Left plot (a): Modelled (black lines) versus measured (green lines) ratios $R_S(\Theta_1)/\bar{R}_{0\xi}$ for different aerosol optical depths at $\lambda=650\text{nm}$. The solid green lines correspond to the two experimentally determined data sets, while the dashed line is the weighted average of both. Right plot (b): The particle size distribution function determined by minimization of the differences between the model and the measurements and presented the same way as in AERONET database, i.e. $dV/d\ln a = a dV/da = (4/3)\pi a^4 \tilde{f}_0(a)$, where dV/da is the particle size volume distribution function and $\tilde{f}_0(a) = \int_0^\infty f(a, h) dh = H_A f_0(a)$ is the columnar particle size number distribution.

bination of smooth log-normal elementary distributions, as defined in Eq. 8. A more precise estimate of this function could be obtained by inverting Eq. 6 using a suitable, but numerically more demanding, regularization procedure.

5 CONCLUSIONS

We demonstrate in this work that the diffuse atmospheric scattered radiance distribution around urban nuclei detected by on-orbit radiometers at night-time contains useful and retrievable information about some key aerosol properties, like the columnar number size distribution function. The method is self-calibrating and does not require the knowledge of the absolute city emissions. This opens the way for more comprehensive studies of the aerosol dynamics at night, improving our knowledge of their characteristics beyond the traditional aerosol optical depth. The results obtained with this approach applied to the radiance data obtained by the VIIRS-DNB radiometer in a particular pass over the city of Zaragoza are presented as a proof-of concept of its feasibility and performance. The DNB band is a panchromatic one, extending from the visible to the NIR. It can be anticipated that the use of multiband radiometry (e.g. RGB calibrated images of night lights acquired from the International Space Station) may provide additional information for a more detailed aerosol characterization.

ACKNOWLEDGEMENTS

This work was supported by the Slovak Research and Development Agency under contract No: APVV-18-0014. Computational work was supported by the Slovak National Grant Agency VEGA (grant No. 2/0010/20). The authors thank Emilio Rodríguez Fernández from Universidade de Santiago de Compostela for his help in locating suitable Suomi-NPP passes over cities, Chris Peat from Heavens-Above by granting permission for reproducing the Suomi-NPP ground track

image, and Juan Ramón Moreta González for kindly providing the data of the AERONET station in Zaragoza. Thanks are also due to the Reviewer for useful suggestions and comments.

REFERENCES

- Cao C., Bai Y., 2014, *Remote Sens.* 6, 11915, doi:10.3390/rs61211915
- Choo G. H., Jeong M. J., 2016, *Korean Journal of Remote Sensing*, 32, 73
- Elvidge C. D., Baugh K., Zhizhin M., Hsu F. C., 2013, *Proceedings of the Asia-Pacific Advanced Network 2013*, 35, 62, doi:10.7125/APAN.35.7
- Elvidge C. D., Baugh K., Zhizhin M., Hsu F. C., Ghosh T., 2017, *International Journal of Remote Sensing* 38, 5860. DOI: 10.1080/01431161.2017.1342050
- Johnson R. S., Zhang J., Hyer E. J., Miller S. D., Reid J. S., 2013, *Atmos. Meas. Tech.* 6, 1245, <https://doi.org/10.5194/amt-6-1245-2013>, 2013
- Kent G. S., Yue G. Y., Farrukh U. O., Deepak A., 1983, *Appl. Opt.* 22, 1655
- Kokhanovsky A. A., 1998, *Journal of the Atmospheric Sciences*. 55, 314
- Kolláth Z., Kránicz B., 2014, *Journal of Quantitative Spectroscopy and Radiative Transfer*, 139, 27
- McHardy T. M., Zhang J., Reid J. S., Miller S. D., Hyer E. J., Kuehn, R. E., 2015, *Meas. Tech.*, 8, 4773. <https://doi.org/10.5194/amt-8-4773-2015>
- Moosmüller H., Ogren J. A., 2017, *Atmosphere* 8, 133
- NASA, 2020, Aerosol Robotic Network (AERONET), https://aeronet.gsfc.nasa.gov/cgi-bin/draw_map_display_aod_v3 (Last accessed, March 13, 2020)
- NOAA, Earth Observation Group, 2019, VIIRS Daily Mosaic, https://ngdc.noaa.gov/eog/viirs/download_ut_mos.html (Last accessed, 20 July 2019)
- Peat C., 2020, Heavens-Above, <https://www.heavens-above.com/> (Last accessed, 15 March 2020)
- Sánchez de Miguel A., Kyba C. C. M., Zamorano J., Gallego J., Gaston K.J., 2019, arXiv:1908.05482 [astro-ph.IM], <https://arxiv.org/abs/1908.05482>
- Wang J., Aegerter C., Xu X., Szykman J. J., 2016, *Atmos. Environ.*, 124, 55–63, 2016.
- Waquet F., Goloub, P., Deuzé J. L., Léon J. F., Auriol F., Verwaerde C., Balois J. Y., Francois P., 2007, *J. Geophys. Res.* 112, D11214
- Zhang J., Reid J. S., Turk J., Miller, S., 2008, *Int. J. Remote Sens.*, 29, 4599
- Zhang J., Jaker S. L., Reid J. S., Miller S. D., Solbrig J., Toth T. D., 2019, *Atmos. Meas. Tech.*, 12, 3209. <https://doi.org/10.5194/amt-12-3209-2019>

This paper has been typeset from a \LaTeX file prepared by the author.